Kirchhoff prestack depth migration in simple models with differently rotated elasticity tensor: orthorhombic and triclinic anisotropy

Václav Bucha
Department of Geophysics, Faculty of Mathematics and Physics, Charles University in Prague, Ke Karlovu 3, 121 16 Praha 2, Czech Republic,
E-mail: bucha@seis.karlov.mff.cuni.cz

Abstract

We use ray-based Kirchhoff prestack depth migration to calculate migrated sections in simple anisotropic homogeneous velocity models in order to demonstrate the impact of rotation of the tensor of elastic moduli on migrated images. The recorded wave field is generated in models composed of two homogeneous layers separated by a curved interface. The anisotropy of the upper layer is orthorhombic or triclinic with the rotation of the tensor of elastic moduli. We apply Kirchhoff prestack depth migration to single-layer velocity models with orthorhombic or triclinic anisotropy with a differently rotated tensor of elastic moduli. We show and discuss the errors of the migrated interface caused by incorrect velocity models used for migration. The study is limited to P-waves.

Keywords

3-D Kirchhoff prestack depth migration, anisotropic velocity model, rotation of the tensor of elastic moduli, general elastic anisotropy, orthorhombic anisotropy, triclinic anisotropy

1. Introduction

It is well known that inaccurate velocity models used for migration can cause position errors of interfaces in migrated sections. Anisotropy-induced distortions in imaging have been analyzed for 2-D transverse isotropic (TI) media (e.g., Larner & Cohen, 1993; Alkhalifah & Larner, 1994) and for transverse isotropic media with a tilted symmetry axis (TTI) (e.g., Ball, 1995; Isaac & Lawton, 1999; Vestrum et al., 1999; Audebert & Dirks, 2006; Behera & Tsvankin, 2009; Vestrum & Lawton, 2010).

To be more close to the real earth structure, velocity models are more often built using anisotropies with lower symmetries. Tsvankin et al. (2010) write that many sedimentary formations including sands and carbonates contain vertical or steeply dipping fracture sets and should be described by effective symmetries lower than TI, such as orthorhombic. Lately, Jones & Davison (2014), in their review on seismic imaging in and around salt bodies, write that several recent case studies have shown improved imaging in the vicinity of salt bodies by taking stress-induced crestal fracturing into account using orthorhombic migration (e.g., Li et al., 2012; Zdraveva et al., 2012).

Jones & Davison (2014) also write that a complete description of anisotropic behavior, combining the layering (TTI) effects with fracture-related effects, in which the fractures could be at arbitrary angles to the TTI polar axis, would be described as triclinic anisotropy. That is well beyond our ability to characterize, however, as we have insufficient information to do so. For microseismic monitoring, Grechka & Yaskevich

(2014) demonstrate the feasibility of joint inversion of field microseismic data for the event locations and an azimuthally anisotropic velocity model containing triclinic layers.

In this paper we continue in ray-based Kirchhoff prestack depth migration studies devoted to position errors of interfaces in migrated sections caused by inaccurate velocity models. We use orthorhombic or triclinic simple velocity models and we study the effect of the rotation of the tensor of elastic moduli (stiffness tensor) on migrated images. The dimensions of the velocity model, shot-receiver configuration, methods for calculation of the recorded wave field and the migration are the same as in the previous papers by Bucha (e.g., 2012, 2013a), where we studied the sensitivity of the migrated images to incorrect anisotropy or to incorrect gradients of elastic moduli. The reason why we use such simple models is to clearly show the influence of one varying parameter on the migrated image, in this case the influence of rotation angle of a rotated elasticity tensor (stiffness tensor). In more complex model with more realistic parameters, it will be very difficult, maybe impossible, to identify causes of errors in migrated images.

We generate synthetic seismograms using the ray theory which is approximate and we apply ANRAY software package (Gajewski & Pšenčík, 1990). To compute the synthetic recorded wave field, we use simple anisotropic velocity models composed of two homogeneous layers separated by one curved interface that is non-inclined in the direction perpendicular to the source-receiver profiles. The anisotropy in the upper layer is orthorhombic or triclinic with the rotation of the tensor of elastic moduli. Both anisotropies are relatively strong. The angles of rotation are equal to 15, 30 and 45 degrees around axes x_1, x_2 or x_3, respectively. Orthorhombic anisotropy has three mutually perpendicular planes of symmetry. Triclinic anisotropy is not mirror symmetric. It is known that the rotation of elasticity tensor causes the change of velocity in specified direction and consequently affects travel times. The rotation of elasticity tensor also causes asymmetry of the orthorhombic anisotropy. The asymmetry influences differently deflection of two-point rays from the vertical plane containing the source-receiver line.

Then we migrate the synthetic data using 3-D ray-based Kirchhoff prestack depth migration in *correct* and *incorrect* single-layer orthorhombic or triclinic velocity models *with* and *without* the rotation of the elasticity tensor. We utilize MODEL, CRT, FORMS and DATA packages (Červený, Klimeš & Pšenčík, 1988; Bulant, 1996; Bucha & Bulant, 2015). The packages used for calculation of the recorded wave field and for the migration are independent.

The distribution of elastic moduli in each *correct* model corresponds to the upper layer of the velocity model (*with* the rotation of the elasticity tensor) in which the corresponding synthetic seismograms have been calculated. We analyze the nearly vanishing part of the migrated interface for *correct* model with triclinic anisotropy rotated around horizontal axis perpendicular to profile lines.

Incorrect models have orthorhombic or triclinic anisotropy *without* the rotation of the tensor of elastic moduli. In this way we simulate situations in which we have made an incorrect guess of the anisotropic velocity model for migration. We display and discuss errors of the migrated interface caused by *incorrect* velocity models used for migration. The calculations are limited to P-waves.

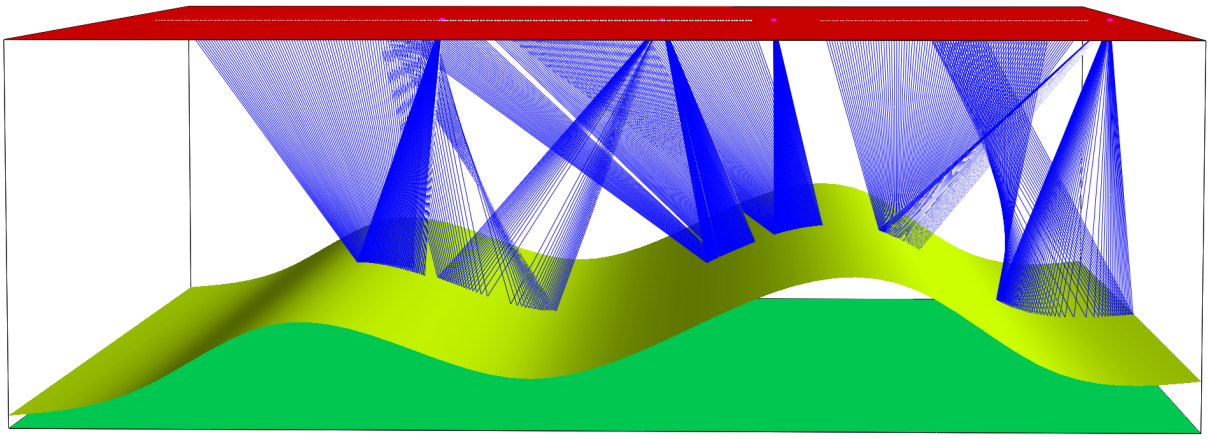

Figure 1. Velocity model with a curved interface. The horizontal dimensions of the velocity model are 0 km $\leq x_1 \leq$ 9.2 km, 0 km $\leq x_2 \leq$ 10 km and the depth is 0 km $\leq x_3 \leq$ 3 km. The velocity model contains one curved interface which is non-inclined in the direction perpendicular to the source-receiver profiles. Two-point rays of the reflected P-wave for one selected profile line (at horizontal coordinate $x_2 = 5$ km) and four shot-receiver configurations (shots 1, 80, 120 and 240 along the profile) are calculated in the velocity model with triclinic anisotropy rotated by 45 degrees around coordinate axis x_2 (TA-X2-45 medium).

2. Anisotropic velocity models

The dimensions of the velocity models and measurement configurations are derived from the 2-D Marmousi model and dataset (Versteeg & Grau, 1991). The horizontal dimensions of the velocity model are 0 km $\leq x_1 \leq$ 9.2 km, 0 km $\leq x_2 \leq$ 10 km and the depth is 0 km $\leq x_3 \leq$ 3 km.

2.1 Velocity models for the recorded wave field

The recorded wave field is computed in the velocity models composed of two homogeneous layers separated by one curved interface (see Figure 1). The curved interface is non-inclined in the direction of the x_2 axis which is perpendicular to the source-receiver profiles. The medium in the upper layer of these velocity models is either orthorhombic or triclinic, with the rotation of the elasticity tensor. The bottom layer is isotropic.

Orthorhombic medium without the rotation (OA) is vertically fractured and is composed of two elements (Schoenberg & Helbig, 1997). The first element, a transversely isotropic background medium with a vertical axis of symmetry (VTI), is fairly typical of many shales. The second element is a set of parallel vertical fractures. Orthorhombic anisotropy has three mutually perpendicular planes of symmetry.

The matrix of density-reduced elastic moduli in km^2/s^2 reads

$$\begin{pmatrix} 9. & 3.6 & 2.25 & 0. & 0. & 0. \\ & 9.84 & 2.4 & 0. & 0. & 0. \\ & & 5.9375 & 0. & 0. & 0. \\ & & & 2. & 0. & 0. \\ & & & & 1.6 & 0. \\ & & & & & 2.182 \end{pmatrix}. \tag{1}$$

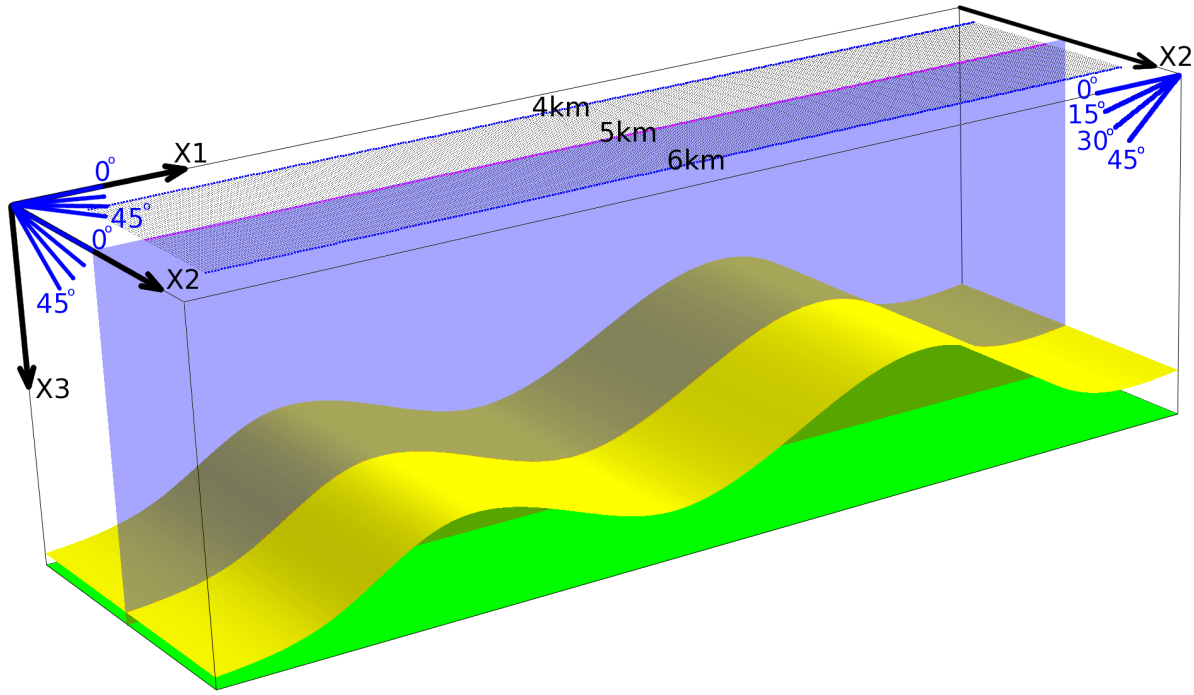

Figure 2. Part of the velocity model with 81 parallel profile lines, the curved interface and the bottom velocity model plane. The horizontal dimensions of the depicted part of the velocity model are 0 km $\leq x_1 \leq$ 9.2 km, 3.5 km $\leq x_2 \leq$ 6.5 km, the depth is 0 km $\leq x_3 \leq$ 3 km. We compute and stack migrated sections in the 2-D plane located in the middle of the shot-receiver configuration, at horizontal coordinate $x_2 = 5$ km. The rotation of the tensor of elastic moduli around axes x_1, x_2 or x_3 is equal to 15, 30 and 45 degrees.

Triclinic medium without the rotation (TA) is represented by dry Vosges sandstone (Mensch & Rasolofosaon, 1997). Triclinic anisotropy is asymmetric.

The matrix of density-reduced elastic moduli in km^2/s^2 reads

$$\begin{pmatrix} 10.3 & 0.9 & 1.3 & 1.4 & 1.1 & 0.8 \\ & 10.6 & 2.1 & 0.2 & -0.2 & -0.6 \\ & & 14.1 & 0. & -0.5 & -1. \\ & & & 5.1 & 0. & 0.2 \\ & & & & 6. & 0. \\ & & & & & 4.9 \end{pmatrix}. \tag{2}$$

For calculation of the recorded wave field we use nine velocity models with the orthorhombic anisotropy and nine velocity models with the triclinic anisotropy, all with differently rotated tensors of elastic moduli in the upper layer (see Figure 2). The angles of the rotation are 15, 30 and 45 degrees around axes x_1, x_2 or x_3. We utilize specific notation for rotated anisotropies, e.g. OA-X1-15 is for the orthorhombic anisotropy rotated 15 degrees around the axis x_1. The rotation of elasticity tensor causes the change of velocity in specified direction and causes asymmetry of the orthorhombic anisotropy. For rotated matrices of density-reduced elastic moduli in Voigt notation refer to Bucha (2014a, 2014b).

The bottom layer in all velocity models is isotropic and the P-wave velocity in the layer is $V_p = 3.6$ km/s. The S-wave velocity is $V_s = V_p/\sqrt{3}$.

2.2 Velocity models for the migration

We migrate in *correct* single-layer velocity models (without the curved interface) with orthorhombic or triclinic anisotropy with the correctly rotated tensors of elastic moduli. The distribution of elastic moduli in *correct* models corresponds to the upper layer of the velocity models (*with* the rotation of the elasticity tensor) in which the synthetic data have been calculated.

Additionally we migrate in *incorrect* single-layer velocity models with orthorhombic or triclinic anisotropy *without* the rotation of the tensor of elastic moduli (matrices (1) and (2)) in order to simulate situations in which we have made an incorrect guess of the anisotropic velocity model for migration.

3. Shots and receivers

The measurement configuration is derived from the Marmousi model and dataset (Versteeg & Grau, 1991). The profile lines are parallel with the x_1 coordinate axis. Each profile line has the following configuration: The first shot is 3 km from the left-hand side of the velocity model, the last shot is 8.975 km from the left-hand side of the velocity model (see Figure 1), the distance between the shots is 0.025 km, and the depth of the shots is 0 km. The total number of shots along one profile line is 240. The number of receivers per shot is 96, the first receiver is located 2.575 km left of the shot location, the last receiver is 0.2 km left of the shot location, the distance between the receivers is 0.025 km, and the depth of the receivers is 0 km. This configuration simulates a simplified towed streamed acquisition geometry.

The 3-D measurement configuration consists of 81 parallel profile lines, see Figure 2. The distance between the parallel profile lines is 0.025 km.

4. Recorded wave field

The recorded wave field in the orthorhombic or triclinic velocity models with the rotation of the tensor of elastic moduli is computed using the ANRAY software package (Gajewski & Pšenčík, 1990). 3-D ray tracing is used to calculate the two-point rays of the reflected P-wave. We then compute the ray-theory seismograms at the receivers.

The recorded wave field is equal for all parallel profile lines, because the distribution of elastic moduli in each layer is homogeneous, and the curved interface is independent of the coordinate x_2 perpendicular to the profile lines (2.5-D velocity model, see Figures 1 and 2).

4.1 Orthorhombic anisotropy

Orthorhombic anisotropy has three mutually perpendicular planes of symmetry. In the case the shot-receiver configuration is in the plane of symmetry (without the rotation of elasticity tensor), the two-point rays stay in the vertical planes corresponding to the individual profiles. The rotation of elasticity tensor causes asymmetry and the two-point rays do not stay in the vertical planes corresponding to the individual profiles even for interfaces non-inclined in the direction perpendicular to the source-receiver profiles. Figures 3 and 4 show the deflection of two-point rays from the vertical plane for selected profile line and selected shot-receiver configurations. We observe the greatest deviation approximately 0.80 km from vertical plane for rotation by 45 degrees around coordinate axis x_1 (the deviation increases with the angle of rotation). The deflection is the smallest for rotations of the elasticity tensor around coordinate axis x_2.

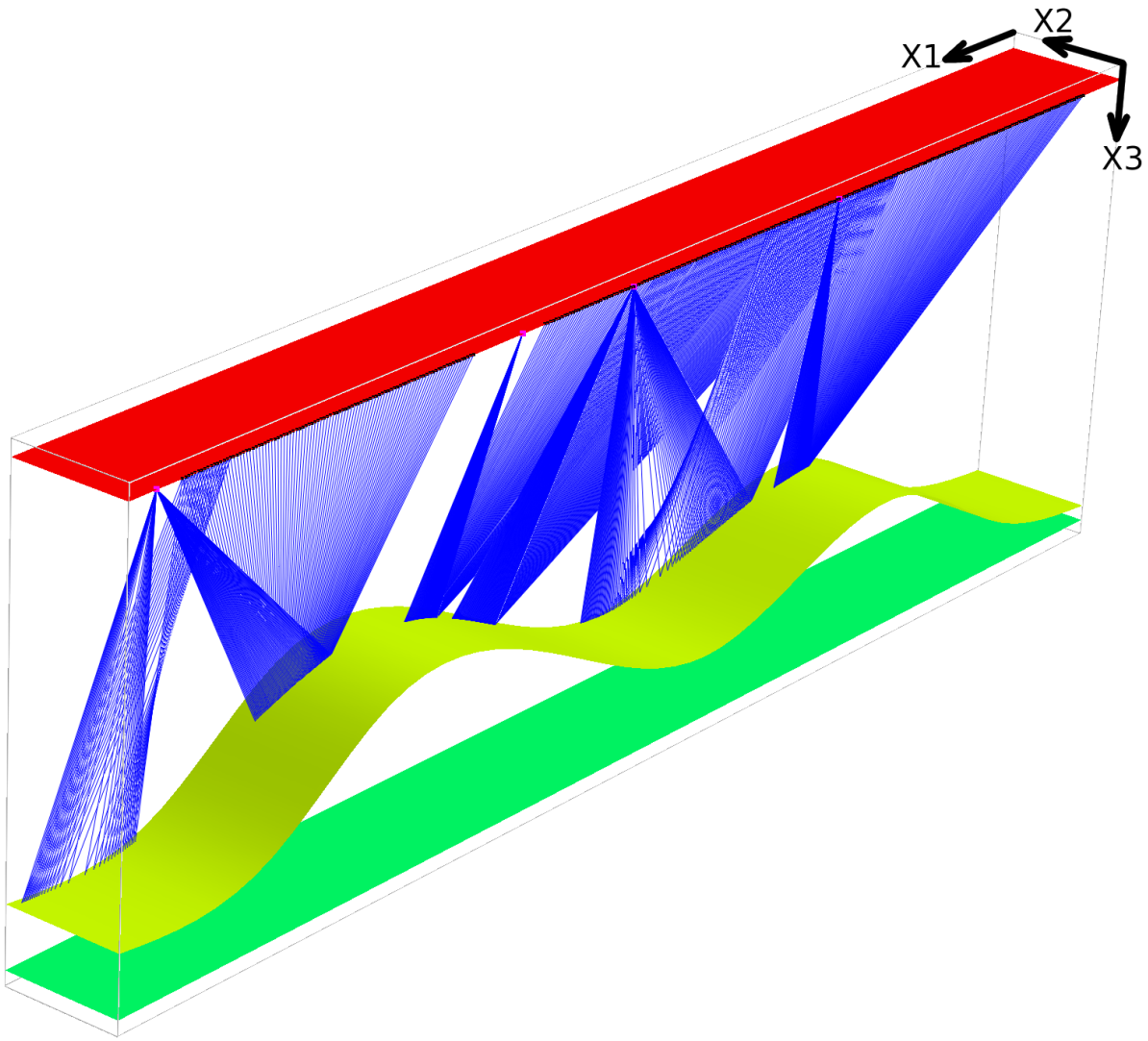

Figure 3. Two-point rays of the reflected P-wave for one selected profile line (at horizontal coordinate $x_2 = 5$ km) and four shot-receiver configurations (from the right-hand side shots 1, 80, 120 and 240 along the profile) are calculated in the velocity model with orthorhombic anisotropy rotated by 45 degrees around coordinate axis x_1 (OA-X1-45 medium). Note that the two-point rays do not stay in the vertical plane corresponding to the profile line. The profile line is situated at top edge of the depicted part of the model (black dots). The maximum deviation of reflections at the curved interface is approximately 0.80 km from vertical plane. The horizontal dimensions of the depicted part of the velocity model are 0 km $\leq x_1 \leq$ 9.2 km, 5.00 km $\leq x_2 \leq$ 5.80 km, the depth is 0 km $\leq x_3 \leq$ 3 km.

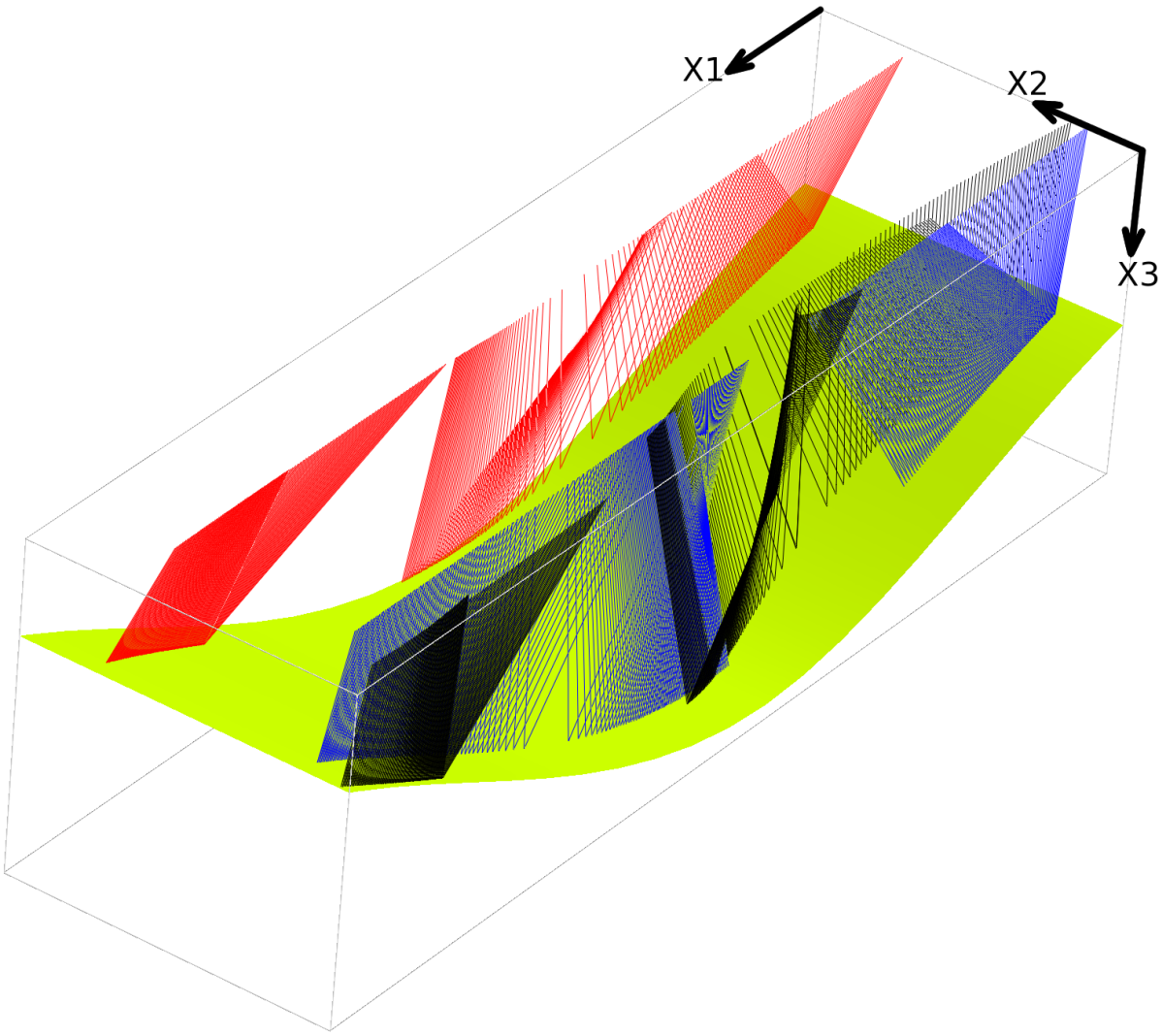

Figure 4. Detailed view of the bottom segments of two-point rays of the reflected P-wave for one shot-receiver configuration (shot 80, profile line at $x_2 = 5$ km). Two-point rays are calculated in three different velocity models with differently rotated orthorhombic anisotropy. The rays of three calculations are displayed together. Red two-point rays correspond to the rotation 45 degrees around coordinate axis x_1 (OA-X1-45 medium), **blue** two-point rays correspond to the rotation 45 degrees around coordinate axis x_2 (OA-X2-45 medium) and **black** two-point rays correspond to the rotation 45 degrees around coordinate axis x_3 (OA-X3-45 medium). The deflection of two-point rays from the vertical plane is the smallest for rotations of the elasticity tensor around coordinate axis x_2 (**blue** rays). The width of the interface in the direction perpendicular to the profile line is approximately 0.95 km (4.85 km $\leq x_2 \leq$ 5.80 km). Note the different paths of reflections at the interface.

The greatest shift (approximately 0.80 km) of the reflection points away from the vertical plane containing the source-receiver line is also visible on cross-sections of the 3-D migrated volume (see Figure 8).

4.2 Triclinic anisotropy

The triclinic asymmetry causes that the two-point rays do not stay in the vertical planes corresponding to the individual profiles. Figures 5 and 6 show the deflection of two-point rays from the vertical plane for selected profile line and selected shot-receiver configurations. We observe the greatest deviation approximately 0.35 km from vertical plane for rotation by 45 degrees around coordinate axis x_1 (the deviation increases with the angle of rotation). The deflection is the smallest for rotations of the elasticity tensor around coordinate axis x_3.

The greatest shift (approximately 0.35 km) of the reflection points away from the vertical plane containing the source-receiver line is also visible on cross-sections of the 3-D migrated volume (see Figure 10).

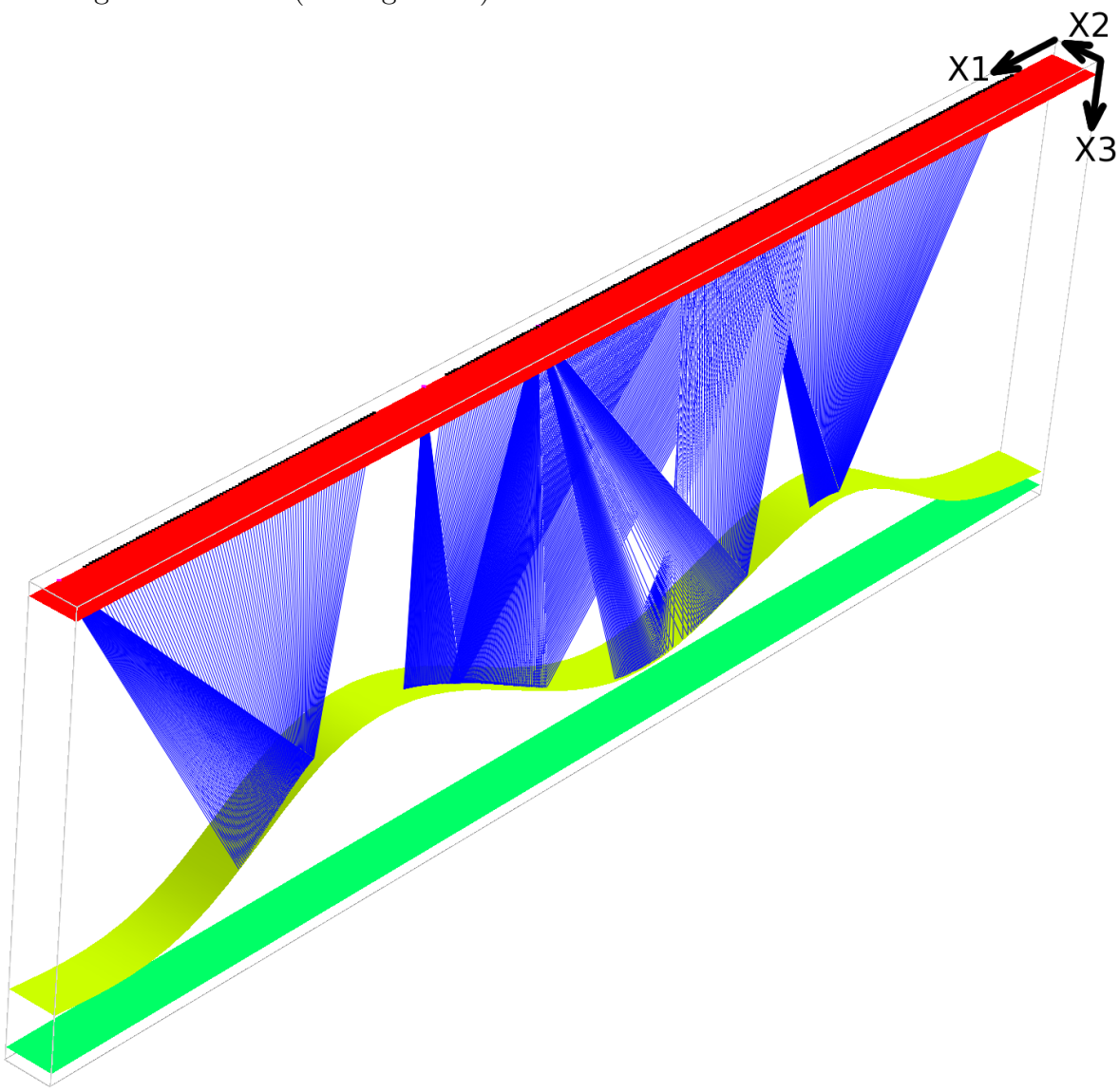

Figure 5. Two-point rays of the reflected P-wave for one selected profile line (at horizontal coordinate $x_2 = 5$ km) and four shot-receiver configurations (from the right-hand side shots 1, 80, 120 and 240 along the profile) are calculated in the velocity model with triclinic anisotropy rotated by 45 degrees around coordinate axis x_1 (TA-X1-45 medium). Note that the two-point rays do not stay in the vertical plane corresponding to the profile line. The profile line is situated at top edge of the depicted part of the model (black dots). The maximum deviation of reflections at the curved interface is approximately 0.35 km from vertical plane. The horizontal dimensions of the depicted part of the velocity model are 0 km $\leq x_1 \leq$ 9.2 km, 4.65 km $\leq x_2 \leq$ 5.00 km, the depth is 0 km $\leq x_3 \leq$ 3 km.

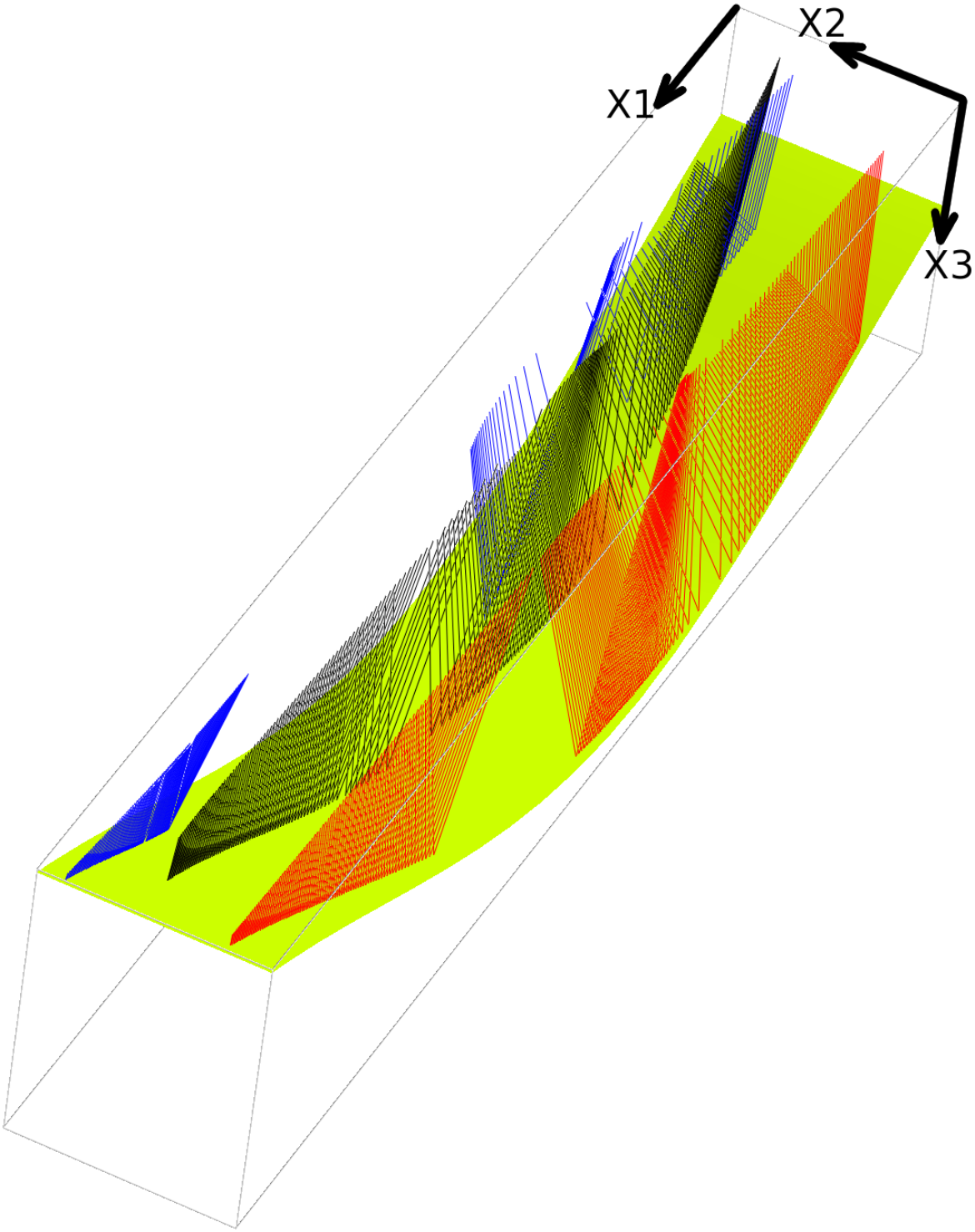

Figure 6. Detailed view of the bottom segments of two-point rays of the reflected P-wave for one shot-receiver configuration (shot 80, profile line at $x_2 = 5$ km). Two-point rays are calculated in three different velocity models with differently rotated triclinic anisotropy. The rays of three calculations are displayed together. Red two-point rays correspond to the rotation 45 degrees around coordinate axis x_1 (TA-X1-45 medium), **blue** two-point rays correspond to the rotation 45 degrees around coordinate axis x_2 (TA-X2-45 medium) and **black** two-point rays correspond to the rotation 45 degrees around coordinate axis x_3 (TA-X3-45 medium). The deflection of two-point rays from the vertical plane is the smallest for rotations of the elasticity tensor around coordinate axis x_3 (**black** rays). The width of the interface in the direction perpendicular to the profile line is approximately 0.51 km (4.66 km $\leq x_2 \leq$ 5.17 km). Note the different paths of reflections at the interface.

5. Kirchhoff prestack depth migration

We use the MODEL, CRT, FORMS and DATA packages for 3-D Kirchhoff prestack depth migration (Červený, Klimeš & Pšenčík, 1988; Bulant, 1996; Bucha & Bulant, 2015). The packages used for calculation of the recorded wave field and for the migration are independent.

The migration consists of two-parametric controlled initial-value ray tracing (Bulant, 1999) from the individual surface points, calculating grid values of travel times and amplitudes by interpolation within ray cells (Bulant & Klimes, 1999), performing the common-shot migration and stacking the migrated images. The shot-receiver configuration consists of 81 parallel profile lines at intervals of 0.025 km (see Figure 2). The first profile line is situated at horizontal coordinate $x_2 = 4$ km and the last profile line is situated at horizontal coordinate $x_2 = 6$ km. For migration we use single-layer velocity models (without the curved interface).

For the purpose of our tests, we calculate only one vertical image section corresponding to the central profile line ($x_2 = 5$ km, see Figure 2). Although only a 2-D line, such an image represents one vertical section of full 3-D migrated volume. We form the image by computing and summing the corresponding contributions (images) from all 81 parallel source-receiver lines. While summing the contributions, the constructive interference focuses the migrated interface and the destructive interference reduces undesirable migration artefacts (non-specular reflections). We also use cosine taper to clear artefacts but some of them especially residual semicircular smiles remain, even when the correct velocity model is used.

5.1 Migration using the correct velocity models

The distribution of elastic moduli in the single-layer velocity model for migration is the same as the distribution in the upper layer of the velocity model (*with* the rotation of the elasticity tensor) used to calculate the recorded wave field.

We perform calculations in *correct* velocity models to demonstrate that the migration algorithm works well. Such migrated sections may be used as a reference for comparison with the migrated sections calculated for *incorrect* velocity models.

5.1.1 Orthorhombic anisotropy

Figure 7 shows stacked migrated section calculated in the *correct* single-layer velocity model with the orthorhombic anisotropy with the rotation of the tensor of elastic moduli around axis x_1 for angle 45 degrees. Migrated sections for rotations around axes x_2 or x_3 and for angles of rotation 15 and 30 degrees are similar and we do not display them (see Bucha, 2014a). The migrated interface is clear and coincides nearly perfectly with the interface in the velocity model used to compute the recorded wave field.

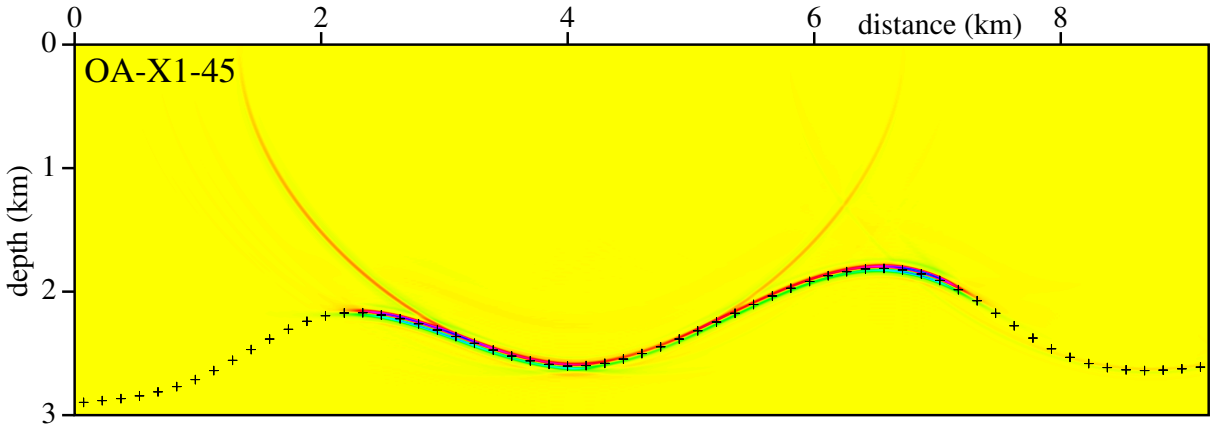

Figure 7. Stacked migrated section calculated in the correct velocity model without interfaces, specified by orthorhombic anisotropy with 45 degree rotation of the tensor of elastic moduli around the x_1 axis (OA-X1-45). The distribution of elastic moduli in the single-layer velocity model for migration is the same as the distribution in the upper layer of the velocity model used to calculate the recorded wave field. 81×240 common-shot prestack depth migrated sections, corresponding to 81 profile lines and 240 sources along each profile line, have been stacked. The crosses denote the interface in the velocity model used to compute the recorded wave field.

Figure 8 shows cross-sections of the 3-D migrated volume corresponding to the profile line at $x_2 = 5$ km. The volume is calculated in the *correct* velocity model with orthorhombic anisotropy rotated by 45 degrees around coordinate axis x_1 (OA-X1-45 medium). The common-shot prestack depth migrated volumes corresponding to 240 sources along the profile line have been stacked. Notice a considerable shift of the stationary point to the left of $x_2 = 5$ km (approximately 0.80 km) on all cross-sections. The shift of reflection points away from the vertical plane is caused by asymmetry of rotated orthorhombic anisotropy. Although the curved interface is non-inclined in the direction perpendicular to the source-receiver profiles, incident and reflected rays do not lie in a vertical plane containing the source-receiver line. This effect is similar to the effect of an inclined interface in an isotropic medium.

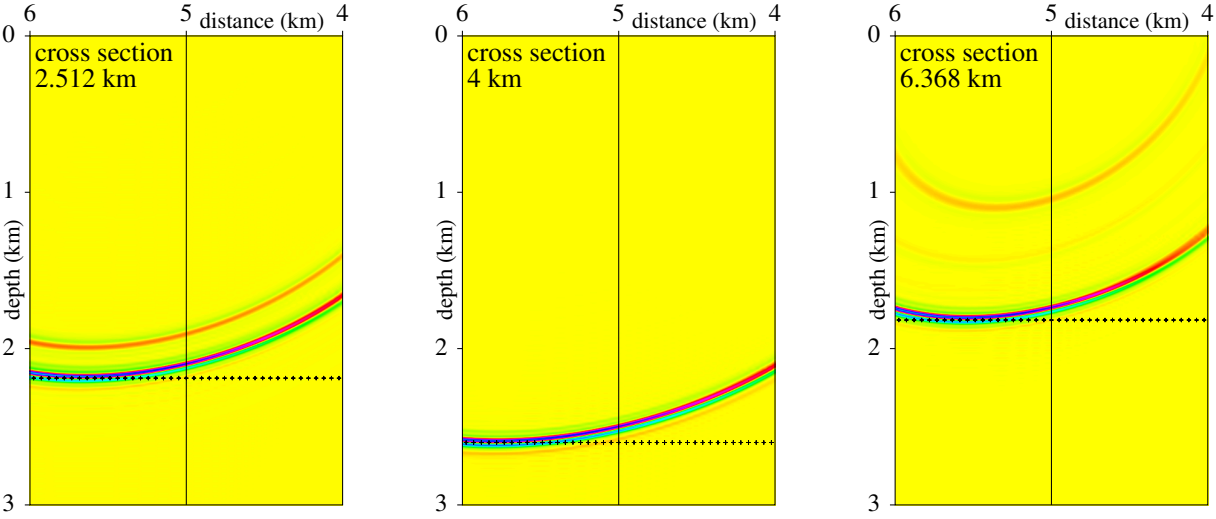

Figure 8. Cross-sections of the 3-D migrated volume corresponding to the line of sources and receivers located at $x_2 = 5$ km. The volume is calculated in the velocity model with orthorhombic anisotropy rotated by 45 degrees around coordinate axis x_1 (OA-X1-45 medium). The common-shot prestack depth migrated volumes corresponding to 240 sources along the profile line have been stacked. Migrated cross-sections (perpendicular to profile lines) are at coordinates $x_1 = 2.512$ km, 4 km, 6.368 km.

5.1.2 Triclinic anisotropy

Figure 9 shows three stacked migrated sections calculated in the *correct* single-layer velocity models with the triclinic anisotropy with the rotation of the tensor of elastic moduli around axes x_1, x_2 or x_3 for angle 45 degrees. Migrated sections for angles of rotation 15 and 30 degrees are similar and we do not display them (see Bucha, 2014b). The migrated interface for rotations around axes x_1 and x_3 is clear and coincides nearly perfectly with the interface in the velocity model used to compute the recorded wave field.

For rotation around the axis x_2 (horizontal axis perpendicular to profile lines) we obtain unexpected results of the migration in *correct* single-layer velocity model. We observe the nearly vanishing part of the migrated interface (see Figure 9b). In all previous studies, sensitivity of the migrated images to incorrect anisotropy or to incorrect gradients of elastic moduli, the migrated interface calculated in the *correct* single-layer velocity models was clear and coincided nearly perfectly with the original interface (see e.g., Bucha, 2012, 2013a). The use of ray method and simple velocity model enable us to clearly explain the phenomenon in the next Section 5.1.2.1.

Figure 10 shows cross-sections of the 3-D migrated volume corresponding to the profile line at $x_2 = 5$ km. The volume is calculated in the *correct* velocity model with triclinic anisotropy rotated by 45 degrees around coordinate axis x_1 (TA-X1-45 medium). The common-shot prestack depth migrated volumes corresponding to 240 sources along the profile line have been stacked. Notice a shift of the stationary point to the right of $x_2 = 5$ km (approximately 0.35 km) on all cross-sections. The shift of reflection points caused by triclinic asymmetry is smaller than for orthorhombic asymmetry (see Figure 8). Even though the curved interface is non-inclined in the direction perpendicular to the source-receiver profiles, incident and reflected rays do not lie in a vertical plane containing the source-receiver line. This effect is similar to the effect of an inclined interface in an isotropic medium.

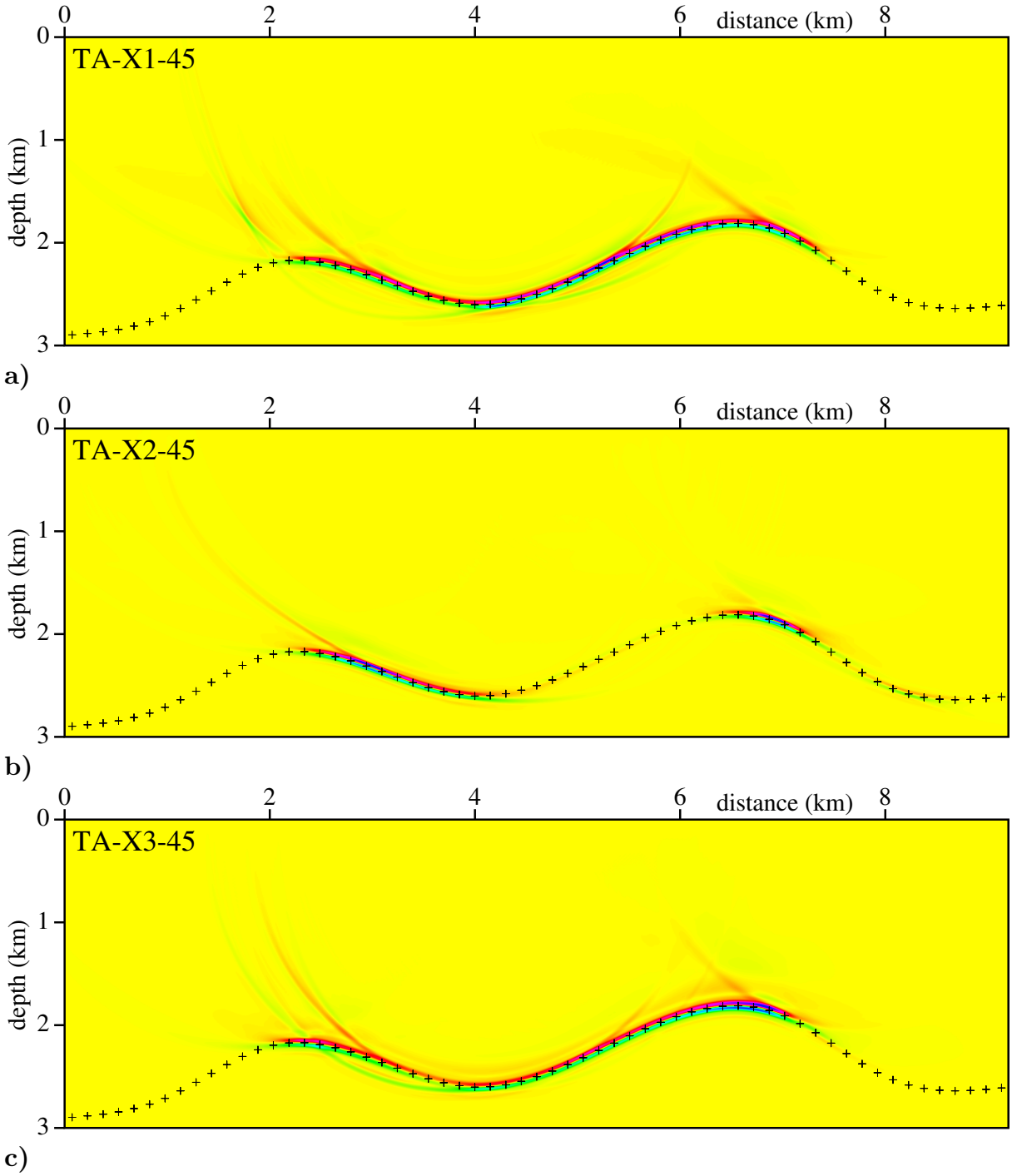

Figure 9. Stacked migrated sections calculated in the correct velocity models without interfaces, specified by triclinic anisotropy with **a)** 45 degree rotation of the tensor of elastic moduli around the x_1 axis (TA-X1-45), **b)** 45 degree rotation of the tensor of elastic moduli around the x_2 axis (TA-X2-45) and **c)** 45 degree rotation of the tensor of elastic moduli around the x_3 axis (TA-X3-45). The distribution of elastic moduli in the single-layer velocity models for migration is the same as the distribution in the upper layer of the velocity models used to calculate the recorded wave field. 81×240 common-shot prestack depth migrated sections, corresponding to 81 profile lines and 240 sources along each profile line, have been stacked. The crosses denote the interface in the velocity models used to compute the recorded wave field.

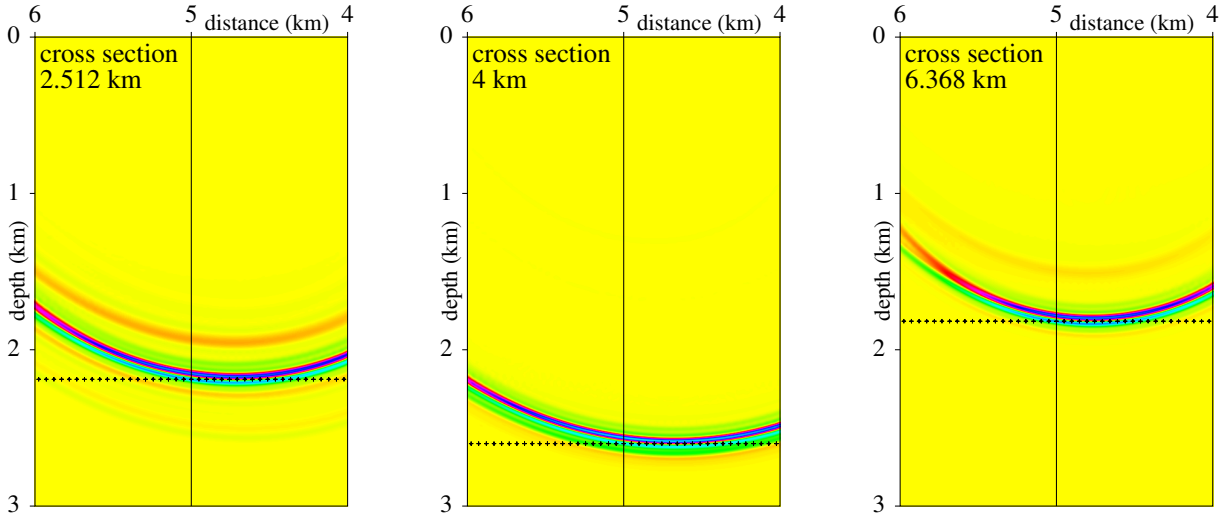

Figure 10. Cross-sections of the 3-D migrated volume corresponding to the line of sources and receivers located at $x_2 = 5$ km. The volume is calculated in the velocity model with triclinic anisotropy rotated by 45 degrees around coordinate axis x_1 (TA-X1-45 medium). The common-shot prestack depth migrated volumes corresponding to 240 sources along the profile line have been stacked. Migrated cross-sections (perpendicular to profile lines) are at coordinates $x_1 = 2.512$ km, 4 km, 6.368 km.

5.1.2.1 Poorly displayed interface in triclinic model

We observed the nearly vanishing part of the migrated interface for rotations around the axis x_2 in *correct* velocity model (see Figure 9b). We identified two causes of the poorly displayed part of the migrated interface.

The **first cause** is obvious from the comparison of the seismograms in Figure 11a and Figure 11b. The seismograms for the model with the rotation in Figure 11b clearly display the change of the sign of the reflection coefficient around a region of the nearly vanishing reflection coefficient. The value of the P-wave velocity in isotropic bottom layer is between the values of the horizontal (axis x_1) and vertical (axis x_3) P-wave velocities in anisotropic upper layer.

The **second cause** of the poorly displayed part of the migrated interface is evident from the comparison of the ray diagrams displayed in Figure 12a and Figure 12b. Note the differences in the illumination of the interface by rays. The illuminated part of the interface is smaller in the model with the rotation of the tensor of elastic moduli.

For more detailed explanation of the nearly vanishing part of the migrated interface refer to Bucha (2013b). We suppose that this migration error may be eliminated by the use of different measurement configuration.

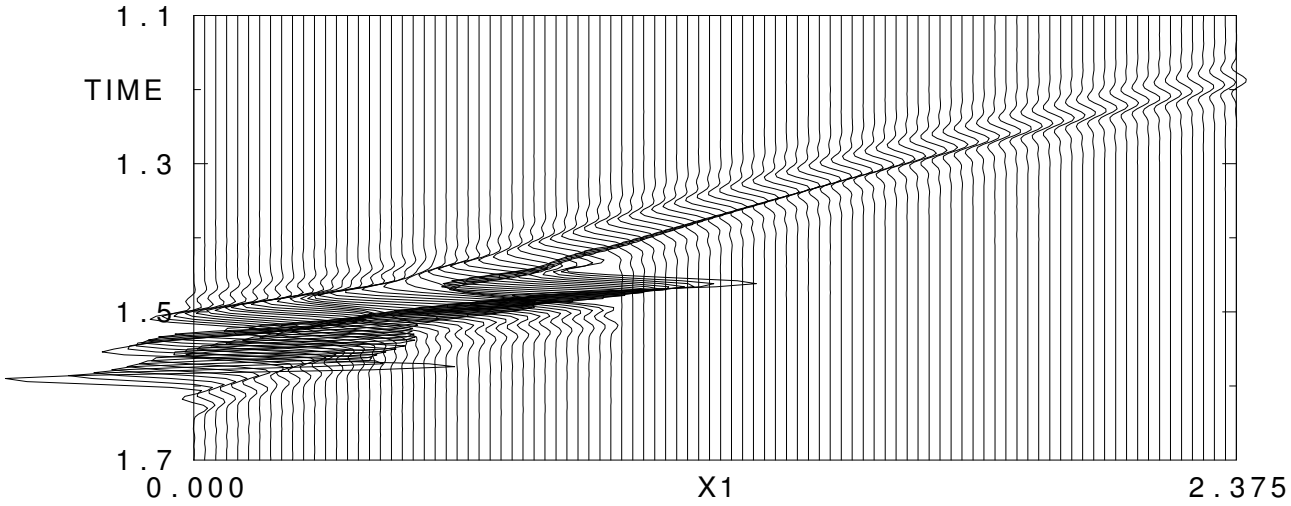

a)

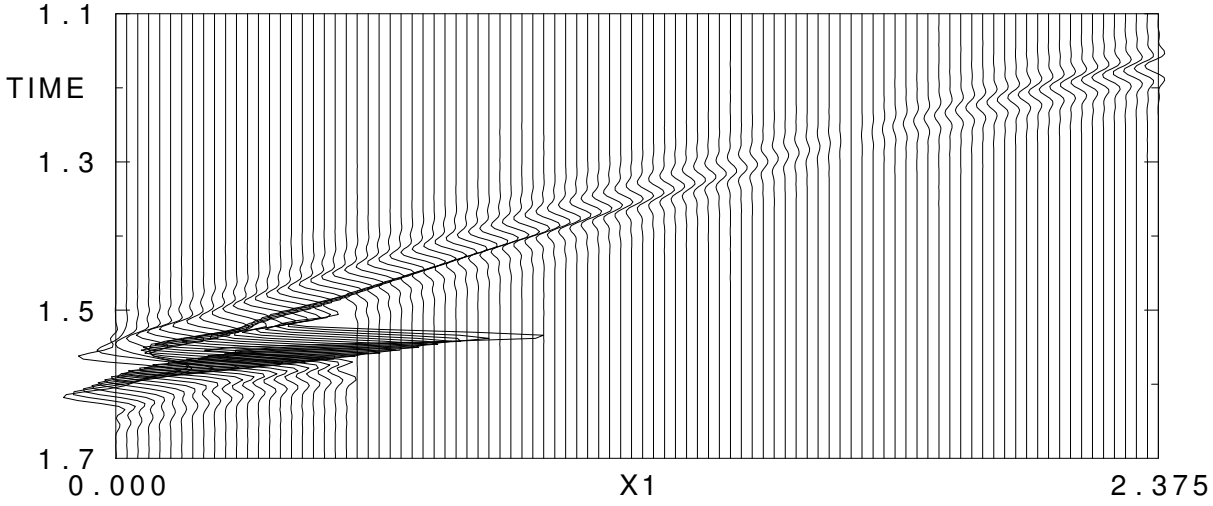

b)

Figure 11. Vertical component of the synthetic seismograms of the reflected P-wave for the single common-shot gather at line $x_2 = 5$ km corresponding to shot 80 ($x_1 = 4.975$ km) calculated in the model with **a)** triclinic anisotropy without the rotation and **b)** triclinic anisotropy with 15 degree rotation of the tensor of elastic moduli around the x_2 axis. Seismograms have the same scaling.

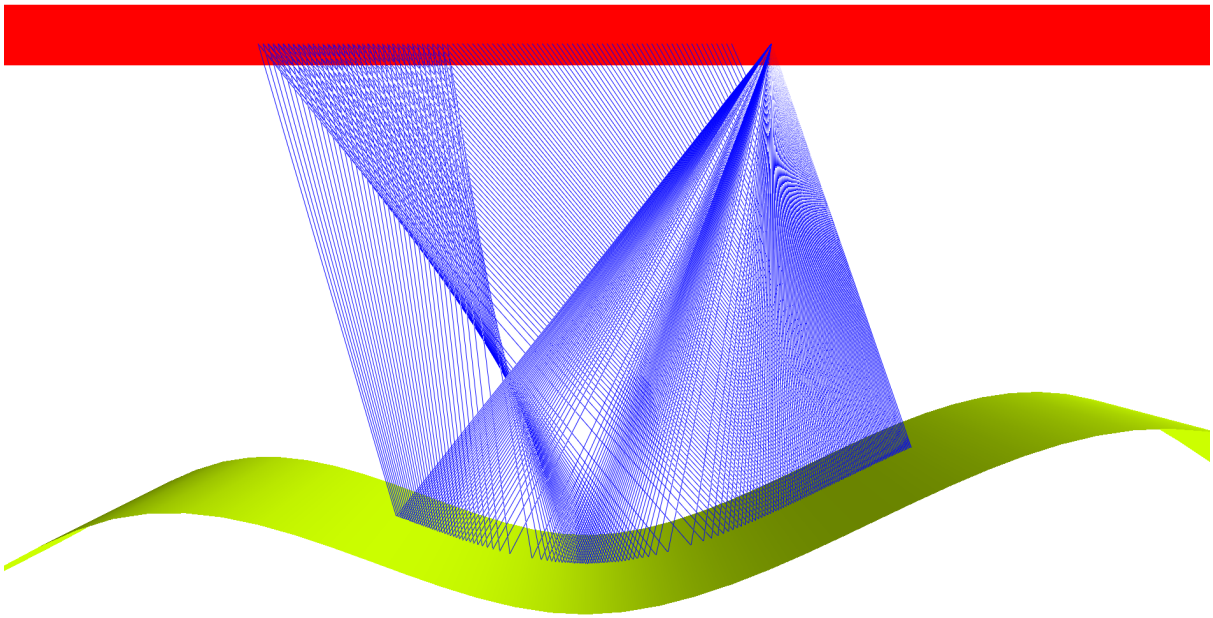

a)

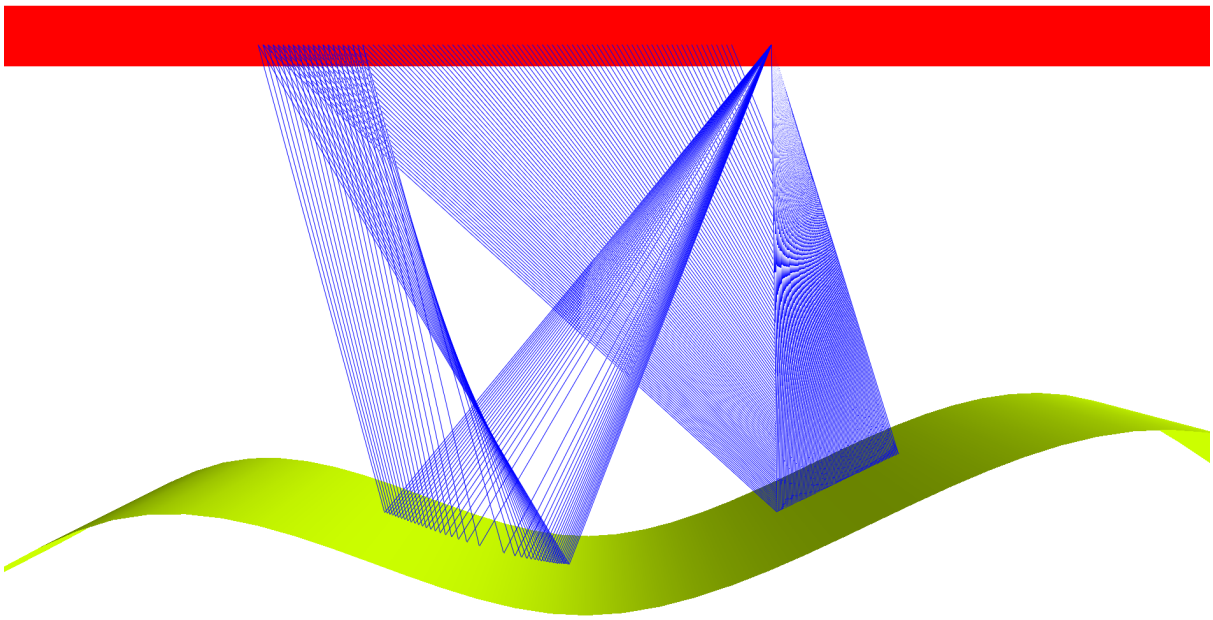

b)

Figure 12. Two-point rays of the P-wave reflected from the curved interface calculated for the single common-shot gather at line $x_2 = 5$ km corresponding to shot 80 ($x_1 = 4.975$ km) in the model with **a)** triclinic anisotropy without the rotation and **b)** triclinic anisotropy with 15 degree rotation of the tensor of elastic moduli around the x_2 axis.

We have already observed nearly the same vanishing part of the migrated interface in *incorrect* velocity models (Bucha, 2012) caused by different phenomena. The poorly displayed part of the migrated interface was caused by the erroneous rotation of single common-shot images. When stacking the common-shot images, this rotation resulted in erasing the mentioned part of the interface due to destructive interference.

5.2 Migration using the incorrect velocity models

In this test, we use Kirchhoff prestack depth migration to calculate migrated sections in *incorrect* homogeneous velocity models. We simulate situations in which we have made an incorrect guess of the rotation of the tensor of elastic moduli around axes x_1, x_2 or x_3. So we migrate in *incorrect* single-layer velocity models with orthorhombic (OA medium) or triclinic (TA medium) anisotropy without the rotation of the tensor of elastic moduli defined by matrices (1) or (2). Residual semicircular smiles in Figures 13 and 14 are migration artifacts caused by the migration method.

5.2.1 Orthorhombic anisotropy

Figure 13 shows three stacked migrated sections for the recorded wave field calculated in models with the orthorhombic anisotropy with the rotation of the tensor of elastic moduli around axes x_1, x_2 or x_3 in the upper layer. Model for migration has the orthorhombic anisotropy without the rotation of the elasticity tensor (OA). We display only migrated sections for the angle of rotation 45 degrees. Results for angles of rotation 15 and 30 degrees are analogous and the errors of migrated interface increase with the angle of the rotation (for migrated sections see Bucha, 2014a).

Figure 13a shows the result of the migration for the recorded wave field calculated in the model with the rotation around axis x_1 (OA-X1-45). The migrated interface is shifted vertically upwards (undermigrated) and the shift increases with the angle of the rotation. This fact indicates that the models with rotated elasticity tensors are faster for reflected P-wave than models without the rotation. Note that the two-point rays are considerably deflected from the vertical plane corresponding to the profile line (see Figure 3). The angle of deflection increases with the angle of the rotation.

Figure 13b displays migrated section for the recorded wave field calculated in the model with the rotation around axis x_2 (OA-X2-45). Note the nearly correctly migrated interface in the horizontal range of approximately $5-6$ km for all angles of the rotation. So the velocity of reflected P-waves for this part of the interface in models with rotated elasticity tensor is nearly the same as the velocity in the model without the rotation. The segments of the interface in horizontal ranges of approximately $2-5$ km and $6-8$ km are defocused and mispositioned (undermigrated), i.e. the velocity of reflected P-waves in models with rotated elasticity tensor is greater than the velocity in the model without the rotation. Surprisingly the two-point rays in this case stay nearly in the vertical plane corresponding to the profile line.

Figure 13c shows stacked migrated section for the recorded wave field calculated in the model with the rotation around axis x_3 (OA-X3-45). The migrated interface is slightly shifted vertically upwards (undermigrated). The shift increases with the angle of the rotation and is noticeable for the angle 45 degrees. Note that the two-point rays do not stay in the vertical plane corresponding to the profile line.

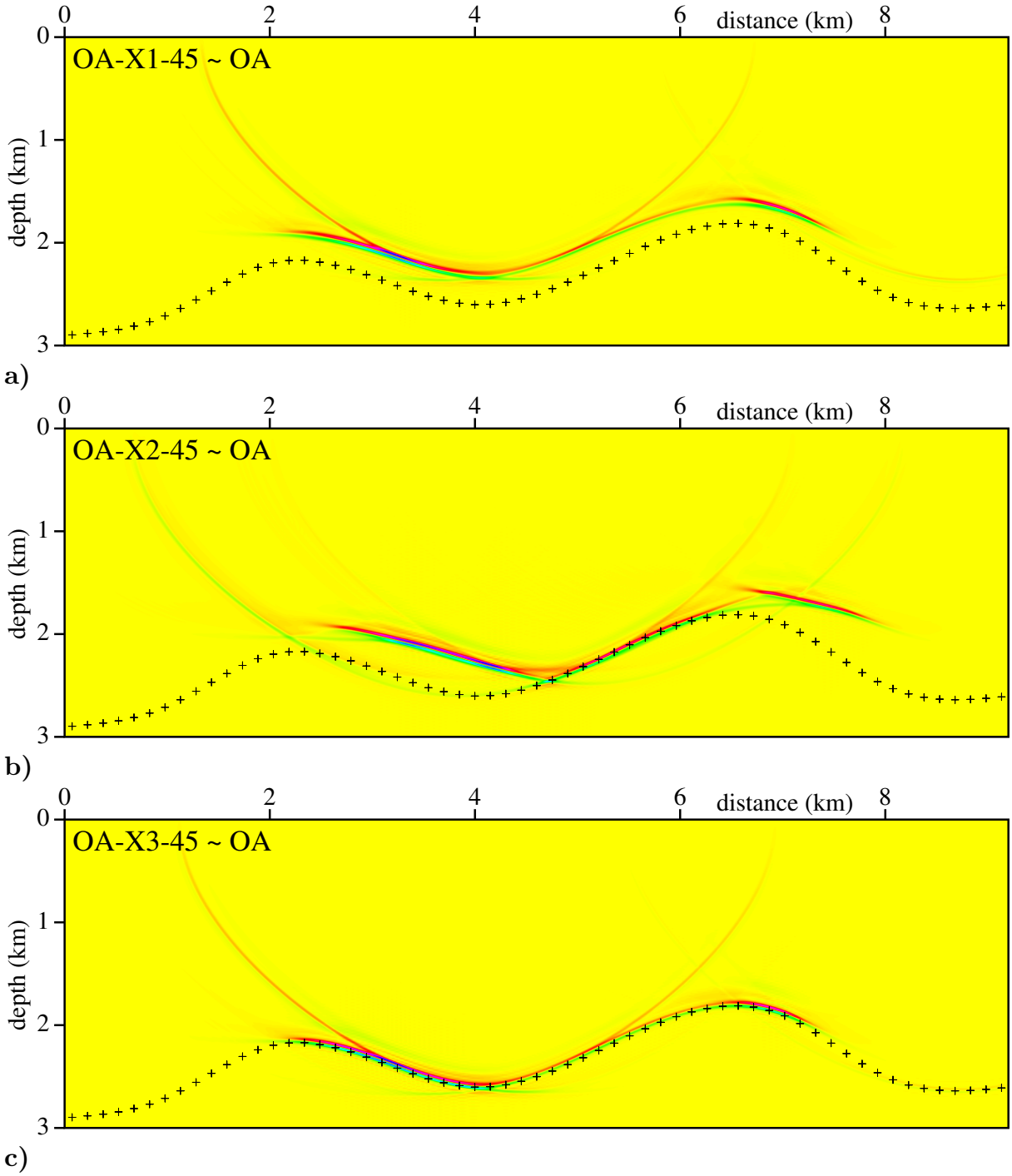

Figure 13. Stacked migrated sections calculated in the incorrect velocity models with orthorhombic anisotropy (OA) without the rotation of the tensor of elastic moduli. The correct anisotropy is orthorhombic with **a)** 45 degree rotation of the tensor of elastic moduli around the x_1 axis (OA-X1-45), **b)** 45 degree rotation of the tensor of elastic moduli around the x_2 axis (OA-X2-45) and **c)** 45 degree rotation of the tensor of elastic moduli around the x_3 axis (OA-X3-45). 81×240 common-shot prestack depth migrated sections, corresponding to 81 profile lines and 240 sources along each profile line, have been stacked. The crosses denote the interface in the velocity models used to compute the recorded wave field.

5.2.2 Triclinic anisotropy

Figure 14 shows three stacked migrated sections for the recorded wave field calculated in models with the triclinic anisotropy with the rotation of the tensor of elastic moduli around axes x_1, x_2 or x_3 in the upper layer. Model for migration has the triclinic anisotropy without the rotation of the elasticity tensor (TA). We display only migrated sections for the angle of rotation 45 degrees. Results for angles of rotation 15 and 30 degrees are analogous and the errors of migrated interface increase with the angle of the rotation (for migrated sections see Bucha, 2014b).

Figure 14a shows the result of the migration for the recorded wave field calculated in the model with the rotation around axis x_1 (TA-X1-45). The migrated interface is slightly shifted vertically downwards (overmigrated) and the shift increases with the angle of the rotation. This fact indicates that the models with rotated elasticity tensors are slower for reflected P-wave than models without the rotation. Note that the two-point rays are deflected from the vertical plane corresponding to the profile line (see Figure 5). The angle of deflection increases with the angle of the rotation.

Figure 14b displays migrated section for the recorded wave field calculated in the model with the rotation around axis x_2 (TA-X2-45). Note the nearly correctly migrated interface in the horizontal range of approximately $4-6$ km for all angles of the rotation. So the velocity of reflected P-waves for this part of the interface in models with rotated elasticity tensor is nearly the same as the velocity in the model without the rotation. The segments of the interface in horizontal ranges of approximately $2-4$ km and $6-8$ km are defocused and mispositioned (overmigrated), i.e. the velocity of reflected P-waves in models with rotated elasticity tensor is lower than the velocity in the model without the rotation. Note that the two-point rays do not stay in the vertical plane corresponding to the profile line.

Figure 14c shows stacked migrated section for the recorded wave field calculated in the model with the rotation around axis x_3 (TA-X3-45). The segments of the interface in horizontal ranges of approximately $2-4$ km and $6-8$ km are slightly defocused and mispositioned (undermigrated), while the interface in the horizontal range of approximately $4-6$ km is nearly correctly migrated. The two-point rays do not stay in the vertical plane corresponding to the profile line. The deflection of rays from the vertical plane is smaller than deflections of rays for rotations around axes x_1 or x_2.

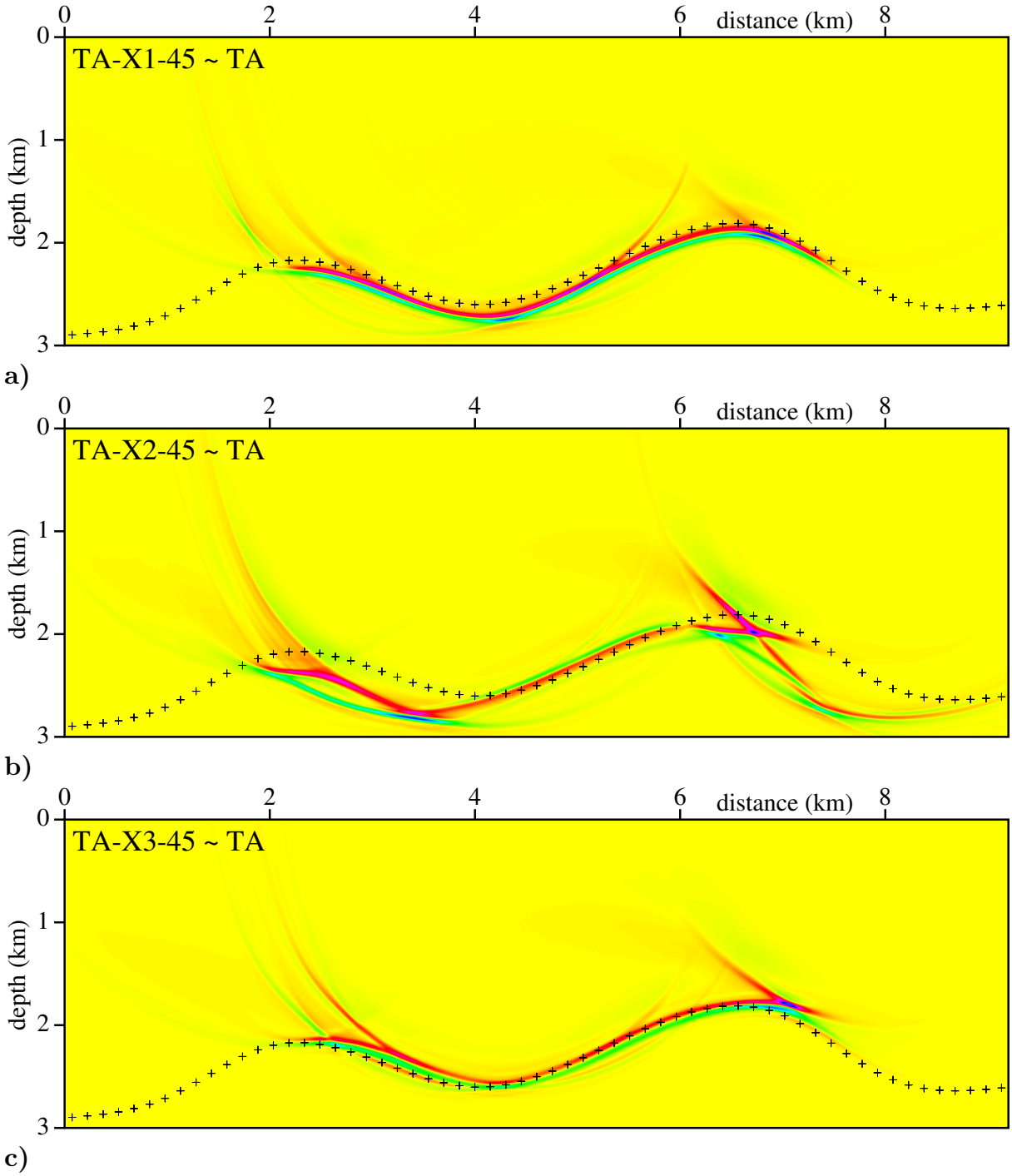

Figure 14. Stacked migrated sections calculated in the incorrect velocity models with triclinic anisotropy (TA) without the rotation of the tensor of elastic moduli. The correct anisotropy is triclinic with **a)** 45 degree rotation of the tensor of elastic moduli around the x_1 axis (TA-X1-45), **b)** 45 degree rotation of the tensor of elastic moduli around the x_2 axis (TA-X2-45) and **c)** 45 degree rotation of the tensor of elastic moduli around the x_3 axis (TA-X3-45). 81×240 common-shot prestack depth migrated sections, corresponding to 81 profile lines and 240 sources along each profile line, have been stacked. The crosses denote the interface in the velocity models used to compute the recorded wave field.

6. Conclusions

In order to study the impact of rotation of the tensor of elastic moduli on migrated images, we generated synthetic seismograms using the ray theory in simple homogeneous two-layer velocity models with orthorhombic or triclinic anisotropy with differently rotated tensors of elastic moduli (stiffness tensors). Both anisotropies are relatively strong. Then we applied 3-D ray-based Kirchhoff prestack depth migration to *correct* and *incorrect* homogeneous single-layer velocity models with orthorhombic or triclinic anisotropy. *Correct* models have anisotropy *with* the correct rotation of the elasticity tensor. *Incorrect* models have anisotropy *without* the rotation and in this way we simulate situations in which we have made an incorrect guess of the rotation of the tensor of elastic moduli. The study has been limited to P-waves.

Calculation of synthetic seismograms showed for some rotations of the elasticity tensor considerable deflection of two-point rays from the vertical plane caused by anisotropic asymmetry. We observed the greatest deviation of two-point rays from vertical plane for both anisotropies for rotation around coordinate axis x_1 (horizontal axis parallel with profile lines).

For migration in *correct* model with orthorhombic anisotropy *with* the rotation of the tensor of elastic moduli around x_1, x_2 or x_3 axes, the migrated interface in the final stacked image coincides nearly perfectly with the interface in the model used to compute the recorded wave field.

In the case of *correct* model with triclinic anisotropy *with* the rotation of the tensor of elastic moduli around axes x_1 and x_3, the migrated interface in the final stacked image coincides nearly perfectly with the interface in the model used to compute the recorded wave field. For rotation around the axis x_2 we observed nearly vanishing part of the migrated interface caused by zero reflection coefficient and phase change decreasing amplitudes of synthetic seismograms, and by worse illumination of the interface by rays. We suppose that this imaging error may be eliminated by the use of different source-receiver configuration. In our previous study of sensitivity of migration to inaccurate anisotropy we observed nearly the same vanishing part of the migrated interface caused by different phenomenon, the erroneous rotation of single common-shot images (Bucha, 2012).

Migration in *incorrect* models with orthorhombic or triclinic anisotropy *without* the rotation of the elasticity tensor showed mispositioning, distortion and defocusing of the migrated interface. The shape of errors of the migrated interface depend on the axis around which we rotate, on rotation angle and on the dip of the interface. We observed for both anisotropies the smallest errors for rotations around the axis x_3 (vertical) and the greatest distortions for rotations around the axis x_2 (horizontal axis perpendicular to the source-receiver profiles). The errors of the migrated interface increase with the angle of the rotation for all rotation axes.

We assume that interaction with other errors caused by incorrect anisotropy, incorrect heterogeneities, incorrect dip and inclination of the interfaces, etc., makes it very difficult to identify specific errors in the images of a real structure.

Acknowledgments

The author thanks Luděk Klimeš and Ivan Pšenčík for their help throughout the work on this paper.

The research has been supported by the Grant Agency of the Czech Republic under Contract 16-05237S, by the Ministry of Education of the Czech Republic within Research Project CzechGeo/EPOS LM2015079, and by the members of the consortium "Seismic Waves in Complex 3-D Structures" (see "http://sw3d.cz").

References

Alkhalifah, T. & Larner, K. (1994): Migration error in transversely isotropic media. *Geophysics*, **59**, 1405–1418.

Audebert, F. & Dirks, V. (2006): TTI anisotropic depth migration: What tilt estimate should we use? 76th Annual International Meeting, SEG, Expanded Abstracts.

Ball, G. (1995): Estimation of anisotropy and anisotropic 3-D prestack depth migration, offshore Zaire. *Geophysics*, **60**, 1495–1513.

Behera, L. & Tsvankin, I. (2009): Migration velocity analysis for tilted transversely isotropic media. *Geophys. Prospect.*, **57**, 13–26.

Bucha, V. (2012): Kirchhoff prestack depth migration in 3-D simple models: comparison of triclinic anisotropy with simpler anisotropies. *Stud. geophys. geod.*, **56**, 533–552.

Bucha, V. (2013a): Kirchhoff prestack depth migration in velocity models with and without vertical gradients: Comparison of triclinic anisotropy with simpler anisotropies. In: *Seismic Waves in Complex 3-D Structures, Report 23*, pp. 45–59, Dep. Geophys., Charles Univ., Prague, online at "http://sw3d.cz".

Bucha, V. (2013b): Kirchhoff prestack depth migration in velocity models with and without rotation of the tensor of elastic moduli: Poorly displayed part of migrated interface in correct model with triclinic anisotropy. In: *Seismic Waves in Complex 3-D Structures, Report 23*, pp. 61–69, Dep. Geophys., Charles Univ., Prague, online at "http://sw3d.cz".

Bucha, V. (2014a): Kirchhoff prestack depth migration in orthorhombic velocity models with differently rotated tensors of elastic moduli. *Seismic Waves in Complex 3-D Structures*, **24**, 59–75, online at "http://sw3d.cz".

Bucha, V. (2014b): Kirchhoff prestack depth migration in triclinic velocity models with differently rotated tensors of elastic moduli. *Seismic Waves in Complex 3-D Structures*, **24**, 77–93, online at "http://sw3d.cz".

Bucha, V. & Bulant, P. (eds.) (2015): SW3D-CD-19 (DVD-ROM). *Seismic Waves in Complex 3-D Structures*, **25**, 209-210, online at "http://sw3d.cz".

Bulant, P. (1996): Two-point ray tracing in 3-D. *Pure appl. Geophys.*, **148**, 421–447.

Bulant, P. (1999): Two-point ray-tracing and controlled initial-value ray-tracing in 3-D heterogeneous block structures. *J. seism. Explor.*, **8**, 57–75.

Bulant, P. & Klimes, L. (1999): Interpolation of ray-theory travel times within ray cells. *Geophys. J. int.*, **139**, 273–282.

Červený, V., Klimeš, L. & Pšenčík, I. (1988): Complete seismic-ray tracing in three-dimensional structures. In: Doornbos, D.J. (ed.), *Seismological Algorithms*, Academic Press, New York, pp. 89–168.

Gajewski, D. & Pšenčík, I. (1990): Vertical seismic profile synthetics by dynamic ray tracing in laterally varying layered anisotropic structures. *J. geophys. Res.*, **95B**, 11301–11315.

Grechka, V. & Yaskevich, S. (2014): Azimuthal anisotropy in microseismic monitoring: A Bakken case study. *Geophysics*, **79**, No. 1, KS1–KS12.

Isaac, J.H. & Lawton, D.C. (1999): Image mispositioning due to dipping TI media: A physical seismic modeling study. *Geophysics*, **64**, 1230–1238.

Jones, I. F. & Davison, I. (2014): Seismic imaging in and around salt bodies. *Interpretation*, **2**, No. 4, SL1–SL20.

Larner, K. & Cohen, J.K. (1993): Migration error in factorized transversely isotropic media with linear velocity variation in depth. *Geophysics*, **58**, 1454–1467.

Li, Y., Han, W., Chen, C. & Huang, T. (2012): Velocity model building for tilted orthorhombic depth imaging. 82nd Annual International Meeting, SEG, Expanded Abstracts.

Mensch, T. & Rasolofosaon, P. (1997): Elastic-wave velocities in anisotropic media of arbitrary symmetry-generalization of Thomsen's parameters ϵ, δ and γ. *Geophys. J. Int.*, **128**, 43–64.

Schoenberg, M. & Helbig, K. (1997): Orthorhombic media: Modeling elastic wave behavior in a vertically fractured earth. *Geophysics*, **62**, 1954–1974.

Tsvankin, I., Gaiser, J., Grechka, V., Baan, M. & Thomsen, L. (2010): Seismic anisotropy in exploration and reservoir characterization: An overview. *Geophysics*, **75**, No. 5, 75A15–75A29.

Versteeg, R. J. & Grau, G. (eds.) (1991): The Marmousi experience. *Proc. EAGE workshop on Practical Aspects of Seismic Data Inversion (Copenhagen, 1990)*, Eur. Assoc. Explor. Geophysicists, Zeist.

Vestrum, R.W., Lawton, D.C. & Schmid, R. (1999): Imaging structures below dipping TI media. *Geophysics*, **64**, 1239–1246.

Vestrum, R. & Lawton, D. (2010): Reflection point sideslip and smear in imaging below dipping anisotropic media. *Geophys. Prospect.*, **58**, 541–548.

Zdraveva, O., Woodward, M., Fowler, P., Nichols, D., & Osypov, K. (2012): Anisotropic model building in complex media: VTI, TTI, or orthorhombic? Presented at SEG/EAGE Summer Research Workshop.